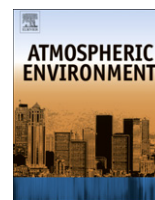




Contents lists available at ScienceDirect

Atmospheric Environment

journal homepage: www.elsevier.com/locate/atmosenv

Regional NO_x emission inversion through a four-dimensional variational approach using SCIAMACHY tropospheric NO₂ column observations

Tianfeng Chai^{a,*}, Gregory R. Carmichael^a, Youhua Tang^a, Adrian Sandu^b,
Andreas Heckel^c, Andreas Richter^c, John P. Burrows^c

^aCenter for Global and Regional Environmental Research, University of Iowa, Iowa City, IA 52242, USA

^bDepartment of Computer Science, Virginia Polytechnic Institute and State University, Blacksburg, VA 24061, USA

^cInstitute of Environmental Physics, University of Bremen, Bremen, Germany

ARTICLE INFO

Article history:

Received 11 November 2008

Received in revised form

5 April 2009

Accepted 26 June 2009

Keywords:

NO₂ column

NO_x emission

Adjoint

Emission inversion

Assimilation

ABSTRACT

In this paper, the NO_x emission scaling factors applied over the 2001 National Emissions Inventory (NEI) are estimated through a four-dimensional variational (4D-Var) approach using SCIAMACHY (Scanning Imaging Absorption spectrometer for Atmospheric CHartography) tropospheric NO₂ columns measured during summer 2004. In the “top-down” approach, two-month average NO₂ columns are assimilated into a regional chemical transport model (CTM), STEM, using different assimilation setups. In a basic setup, NO_x emissions are adjusted by assimilating the NO₂ columns. A more general setup of emission inversion allows the initial O₃ concentrations be adjusted along with the NO_x emissions. A final case is set up to assimilate both the NO₂ columns and O₃ measurement from various platforms while allowing adjustments of both the NO_x emissions and the initial O₃ concentrations. It is found that the addition of O₃ measurements did not improve the NO_x emission inversion. With the NO_x emission at surface and upper levels being adjusted separately, results from four cases show that the elevated NO_x emission reduction ranges from 8.9% to 11.4%, and the surface NO_x emission reduction is up to 6.6%. All the cases show NO_x emission reduction in Ohio valley and Washington, District of Columbia areas.

© 2009 Elsevier Ltd. All rights reserved.

1. Introduction

As the most important ozone precursor and a direct contributor to the local air pollution itself, nitrogen dioxide (NO₂) is one of the key species in atmospheric chemistry of earth's troposphere. Measurements by satellite instruments Global Ozone Monitoring Experiment (GOME, from August 1995 to June 2003) spectrometer (Burrows et al., 1999) and Scanning Imaging Absorption spectrometer for Atmospheric CHartography (SCIAMACHY, since August 2002) (Bovensmann et al., 1999) provide continuous global coverage of NO₂ columns. Richter and Burrows (2002) presented a technique using the Differential Optical Absorption Spectroscopy (DOAS) to retrieve the tropospheric NO₂ columns from the GOME satellite measurements. By applying the technique to GOME and SCIAMACHY observations from 1995 to 2004, Richter et al. (2005) found significant reductions of tropospheric NO₂ over parts of Europe and over the Ohio valley region in the USA. An upward

trend of tropospheric NO₂ over the years was observed over parts of China and in the northeast of the USA.

To a first approximation, the changes of tropospheric NO₂ columns reflect the NO_x emission changes. However, transport and photochemical reactions that affect NO₂/NO_x partitioning have to be taken into account in order to attribute the changes in NO₂ levels to changes in emissions. The nonlinear relationship between NO_x emissions and NO₂ columns was demonstrated by Stavrou et al. (2008). Using the IMAGES global CTM and its adjoint along with the GOME/SCIAMACHY observations, they showed that the inferred emission growth rate in Beijing region from 1997 to 2006 as $\approx 9\%$ year⁻¹ in both summer and winter although there is dramatic differences in the growth rate of the observed NO₂ columns between the two seasons (5.3% year⁻¹ in summertime and 11.8% year⁻¹ in wintertime). Therefore, to infer the emission of NO_x via the “top-down” approach, it is important to fully take advantage of the CTMs which have our best understanding of the physical and chemical processes thoroughly implemented.

Emission inversion problems have drawn a lot of attention in recent years. For instance, Pétron et al. (2002) constrained the global emissions of carbon monoxide (CO) by using a three-dimensional inverse modeling scheme with the IMAGES model. Palmer et al. (2003) and Wang et al. (2004) used aircraft and surface

* Corresponding author. Now at Science and Technology Corporation, Hampton, VA 23666, USA, on assignment to NOAA Air Resources Lab, Silver Spring, MD 20910, USA.

E-mail address: tianfeng.chai@noaa.gov (T. Chai).

station observations of CO and NO_y during the Transport and Chemical Evolution Over the Pacific (TRACE-P) mission in combination of an optimal estimation inverse model to constrain the regional CO and NO_x emissions of different sources. Space-based observations of NO₂ columns have been utilized to constrain NO_x emissions over both global and regional scales using different methods (Martin et al., 2003; Jaeglé et al., 2005; Boersma et al., 2008; Napelenok et al., 2008). Recently, some CTMs and their adjoints have been utilized in the “top-down” emission estimations. The IMAGES global CTM and its adjoint were used to invert CO and NO_x emissions with both surface and satellite observations (Müller and Stavrou, 2005; Stavrou and Müller, 2006; Stavrou et al., 2008). The STEM regional CTM and its adjoint model were developed for emission inversion problems and were applied to analyze the black carbon (Hakami et al., 2005) and mercury (Pan et al., 2007) emission inventories using the observations during the Asian Pacific Regional Aerosol Characterization Experiment (ACE-Asia). Henze et al. (2008) developed an inverse modeling scheme for PM_{2.5} precursor emissions using the adjoint of GEOS-Chem.

In this study, we use the SCIAMACHY tropospheric NO₂ columns during the International Consortium for Atmospheric Research on Transport and Transformation (ICARTT) (Singh et al., 2006) operations in the summer of 2004 and the STEM regional CTM to deduce time-independent scaling factors applied to grid-based NO₂ emissions generated using the 2001 U.S. EPA National Emissions Inventory (NEI). In the emission inversion, two separate sets of emission scaling factors are applied to surface and elevated NO_x emissions, respectively. A general setup of emission inversion that also allows the adjustment of initial concentrations of chemical species is also tested. In addition, the effect of assimilating ozone observations from various platforms is discussed.

The paper is organized as follows. Section 2 describes the SCIAMACHY data. A brief description of the STEM model and the emission inversion method using the variational approach is given in Section 3. Section 4 presents the emission inversion results. A summary is given in Section 5.

2. SCIAMACHY tropospheric nitrogen dioxide observations

The tropospheric NO₂ columns from SCIAMACHY used in this study were prepared at the Institute of Environmental Physics, University Bremen, Germany for the ICARTT project. As the sensitivity of nadir measurements decreases strongly towards the surface, the NO₂ retrieval requires the knowledge of the vertical

profile shape (Richter and Burrows, 2002). For the SCIAMACHY NO₂ column retrievals, daily MOZART (Horowitz et al., 2003) model profiles were used for the air mass factors (AMF) calculation. Our current STEM model runs used the same MOZART profiles to provide boundary conditions. Thus, integrating the NO₂ mass over the model layers without averaging kernels generates comparable NO₂ columns.

Although SCIAMACHY can provide global coverage of NO₂ columns, the region of our interest is only partially covered each day. Fig. 1(a) shows the observed regions on July 20, 2004. The observing time is around 1030 local time. To eliminate the effect of clouds on the retrievals, a simple criterion, the normalized intensity < 0.15, was used to select cloud-free regions. Fig. 1(b) shows the tropospheric NO₂ columns on July 20, 2004 after removing the cloud regions. The number of measurements is significantly reduced after the cloud removal. Hereafter, only data associated with the normalized intensity less than 0.15 are used.

For the NO₂ columns shown in Fig. 1, not all the NO_x emissions will be constrained if only such spatially incomplete samplings are incorporated in the emission inversion. To have a better constraint from the measurements in the “top-down” emission inversion, it is desirable to have a near complete sampling throughout the domain. Here we chose to merge the available NO₂ columns from July 1 to August 31, 2004 together by neglecting the daily variations.

Fig. 2 shows the cloud-free measurements during the weekends and weekdays from July 1 to August 31, 2004, respectively. Even with the data of 18 different weekends stacked together, there are still significant blank regions. Merging the 44 weekdays generates a much better coverage of the domain, although there are still areas left without observations, e.g., middle Pennsylvania. However, these areas are well represented by the data during the weekends. Fig. 2 also shows little contradictions between measurements from different days. Both weekday and weekend data sets show strong and similar spatial patterns revealing the various levels of anthropogenic activities at different locations. There are slight differences between the data sets of weekdays and weekends, but the differences are relative small compared with the spatial variations. In order to achieve a complete spatial coverage in the domain, we stacked both weekday and weekend data together. Such merging also helps to eliminate the effect of daily variation in NO_x emission, which is not of our interest here.

After stacking all the data together, we calculated the mean and standard deviation of the observations inside each grid cell. Whether a measurement is inside a grid cell is decided by the

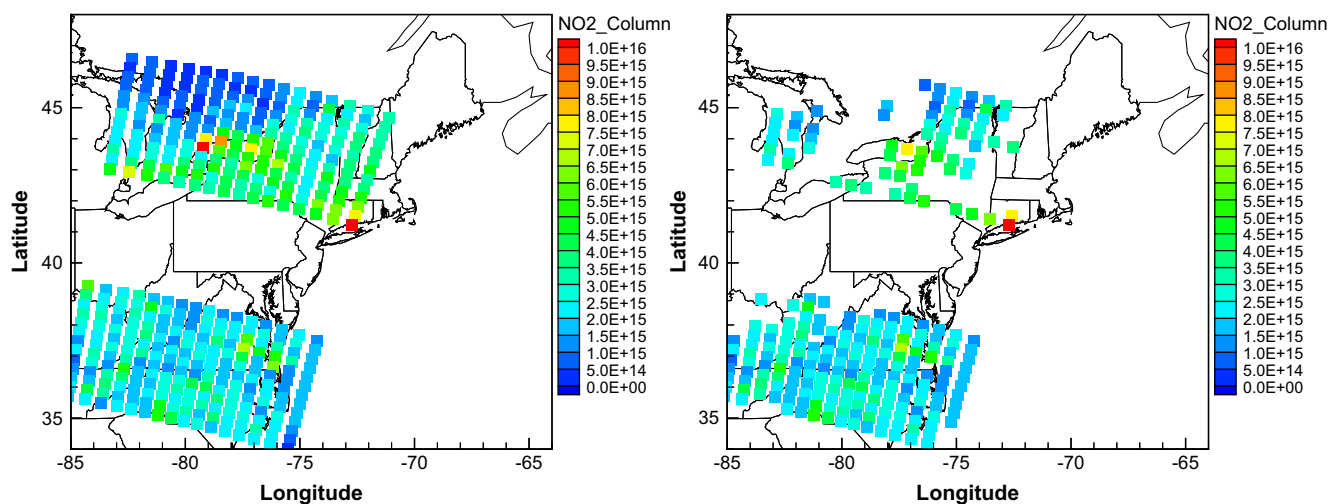


Fig. 1. SCIAMACHY NO₂ columns on July 20, 2004. Unit: molecules cm⁻². Original data shown on the left (a); data with the normalized intensity less than 0.15 shown on the right (b).

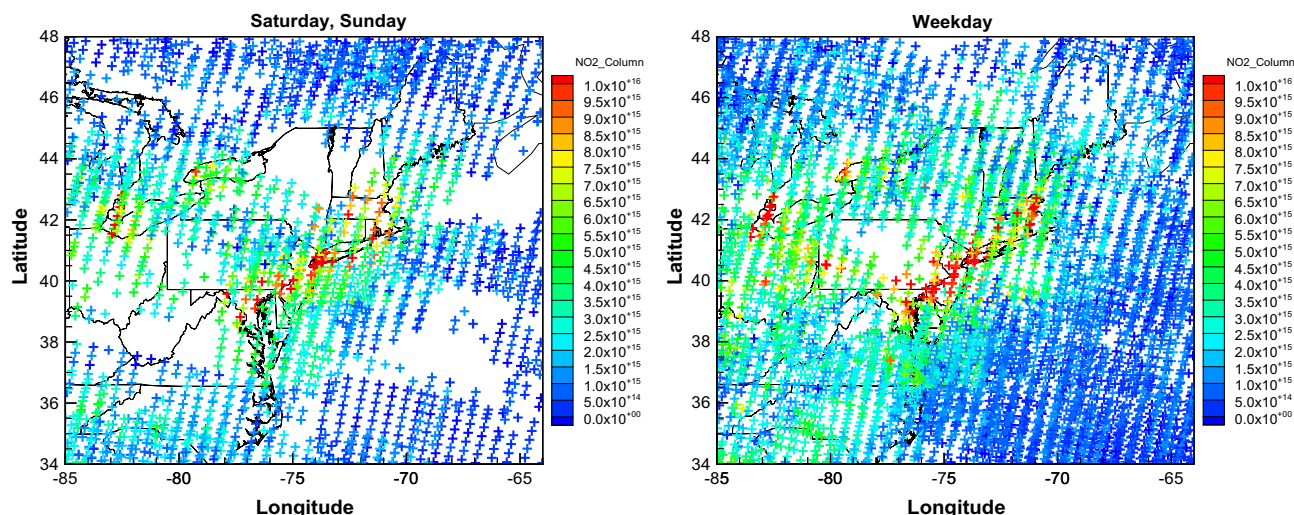


Fig. 2. SCIAMACHY NO₂ columns from July 1 to August 31, 2004. Unit: molecules cm⁻². Left: accumulated data during the weekends. Right: accumulated data during the weekdays.

center of the pixel. The standard deviation was then normalized by the local mean to indicate the variation of the observation in the two-month period. Fig. 3 shows the distributions of the mean observations and normalized standard deviation in the computational domain. For 90.4% of the grid cells, the normalized standard deviation is smaller than 70%. Except for the New York City area, the locations with large variations are often associated with low NO₂ columns. Note that the deviations inside each grid cell not only come from the daily variations, but also come from the spatial variations not resolved by the model. The footprint of a SCIAMACHY pixel is approximately 60 × 30 km², i.e., about half of the 60 × 60 km² model grid cell. Thus, the standard deviations calculated inside grid cells include the representative errors. As Fig. 2 shows little variation between days and the daily variation is not of our interest here, we generate a pseudo-observation data set that has the two-month mean NO₂ column at each grid cell as the measurement value. The normalized standard deviation at each grid cell reflects the uncertainty of the pseudo-observation and is assigned as the uncertainty of the pseudo-observations. Fig. 3 shows the normalized standard deviation is close to 50% for most

of the domain (81% of grid cells fall between 30% and 70%). In addition, the average measurement time during the day inside each grid cell was given to the pseudo-observation and it is used by the model to reconstruct the NO₂ columns. Note that it is difficult to give a good estimate of the NO₂ column retrieval uncertainty. If the SCIAMACHY retrieval uncertainty is not significantly greater than 50%, as most pseudo-observation uncertainties are close to, including the retrieval uncertainty is not expected to add more uncertainties to the pseudo-observation uncertainties.

3. Method

3.1. Chemical transport model

In this study, the STEM-2K3 (Tang et al., 2004) regional chemical transport model is employed. It is a flexible regional-scale chemical transport model using SAPRC99 chemical mechanism (Carter, 2000) with on-line photolysis solver (Tang et al., 2003). Meteorological inputs to the model came from the fifth-generation Mesoscale Model (MM5) using NCEP (National Centers for Environmental

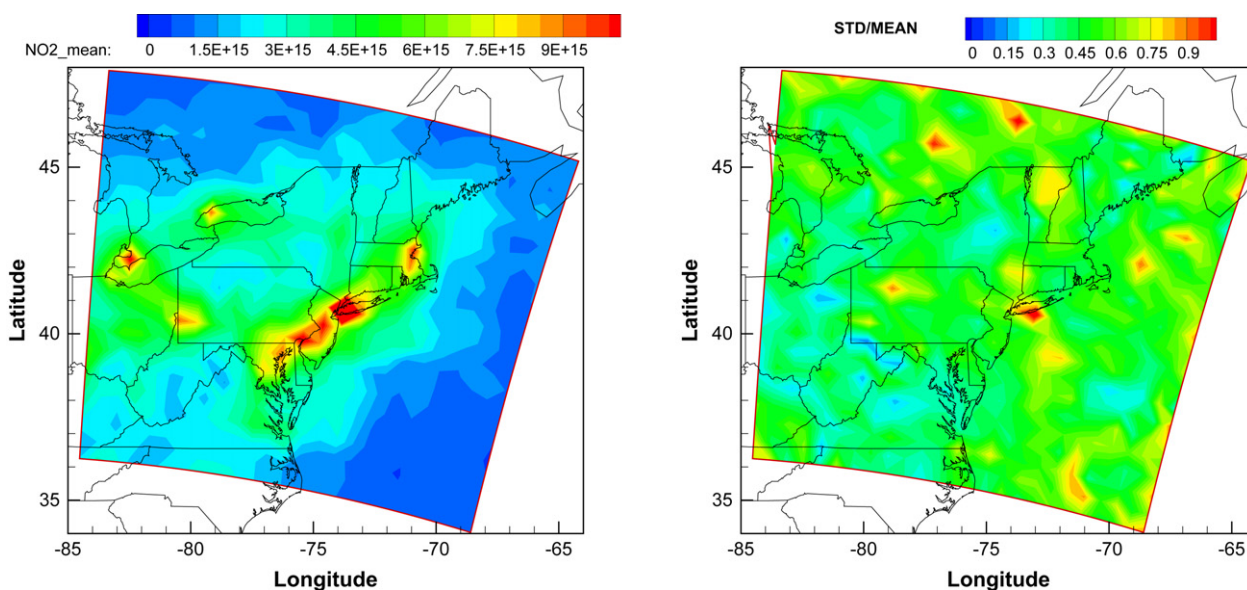


Fig. 3. Mean (left, Unit: molecules cm⁻²) and normalized standard deviation (right, STD/mean) of SCIAMACHY NO₂ columns from July 1 to August 31, 2004.

Prediction) FNL (Final Global Data Assimilation System) analyzed data during post-analysis. A grid with a 60 km horizontal resolution (25 cells in longitude, and 22 cells in latitude) is used over the northeast US domain, as shown in Fig. 3. Vertically the model had 21 layers, extending from the surface to 100 hPa using 0.999, 0.9965, 0.9925, 0.985, 0.97, 0.945, 0.91, 0.87, 0.825, 0.77, 0.71, 0.65, 0.59, 0.53, 0.47, 0.41, 0.35, 0.285, 0.21, 0.125, and 0.04 in sigma coordinates. The emissions inventory was based on the 2001 NEI, with updated large point source emissions (Frost et al., 2006). Upper troposphere lightning NO_x emissions were added to the model based on the National Lightning Detection Network (NLDN), modulated by signal strength and multiplicity of flashes. Further information about the lightning emissions can be found in Tang et al. (2007). Biogenic emissions were estimated using Biogenic Emissions Inventory System 2 (BEIS2) which generates time-varied isoprene and monoterpene emissions driven by meteorological variables from MM5. Forest fires that occurred during the ICARTT period were largely outside the model domain (in Alaska and Northwestern Canada), therefore their influence was incorporated through lateral boundary conditions from MOZART global chemical model predictions. The boundary conditions are provided by STEM-2K3 run over a bigger domain that covers the continental United States (see Tang et al., 2007 for detail).

The evolution of the chemical constituent concentration vector c in time (t) can be described as

$$\frac{\partial c}{\partial t} = -u \cdot \nabla c + \frac{1}{\rho} \nabla \cdot (\rho K \cdot \nabla c) + \frac{1}{\rho} f + E \quad (1)$$

Here we denote by u the wind field vector, ρ the air density, K the turbulent diffusivity tensor, f the chemical transformation rate, and E the emission rate.

3.2. Emission inversion via 4D-Var

In this study, the emission inversion problem is solved via the STEM 4D-Var system (Sandu et al., 2005; Chai et al., 2006, 2007). The discrepancy between the available observations and model counterparts is built into a cost functional. Optimal solutions of model parameters such as the NO_x emissions are obtained by finding new parameters which minimize the cost functional. To solve the minimization problems efficiently, the sensitivity of the cost functional with respect to the control variables (parameters to

be adjusted) need to be calculated. Adjoint models provide the most efficient way to calculate the gradients of a scalar cost functional with respect to a large number of control variables (Tala-Grand and Courtier, 1987).

The cost functional J is defined as

$$J = \frac{1}{2}[\varepsilon - 1]^T E^{-1}[\varepsilon - 1] + \frac{1}{2}[c_0 - c_b]^T B^{-1}[c_0 - c_b] + \frac{1}{2}[y - h(c)]^T O^{-1}[y - h(c)] \quad (2)$$

E , B , and O are error covariance matrices for emission scaling factors ε , a priori (background) initial states c_b , and observations in discrete spaces, respectively. h is a projection operator, calculating the observation vector y from the model space c . In the current study the control variables can include both initial states c_0 and emission rates. The subscript “0” is used to denote variables at the instant $t = 0$. Assuming that the operator h is linear, $h(c)$ can be written as $h(c) = H \cdot c$. In our application, H reflects vertical integration and linear interpolation in time when constructing model counterparts of the NO₂ columns at the same measurement time.

A larger-scale bound-constrained limited-memory quasi-Newton code, L-BFGS-B (Zhu et al., 1997) is used for the minimization. The maximum number of iterations is set to be 25. Tests that add 25 extra iterations show little improvements in cost functional reduction. The initial O₃ background error covariance B were estimated using both NMC and observational methods. Truncated singular value decomposition (SVD) regularization is used for the inversion of B matrix (see Chai et al., 2007 for detail). Assuming uncorrelated emission scaling factor errors in space, the uncertainty of emission scaling factor ε was chosen as 0.5 uniformly. The upper and lower bounds of ε during the minimization with L-BFGS-B subroutine were assigned as 10 and 0.1, respectively. The observation errors of NO₂ pseudo-columns were given by the standard deviations at individual grid cells during the two-month period. Following Chai et al. (2007), the observation errors of O₃ were set to be 8 ppbv everywhere. Errors of NO₂ pseudo-columns and O₃ observations were assumed uncorrelated among themselves and between each other.

The assimilation time window is chosen to be 24 h for the following emission inversion cases. We first started our emission inversion tests by only adjusting the NO_x emission rates. Later we included the initial ozone concentrations as control variables as well. It is designed to eliminate the effect of the notable errors in

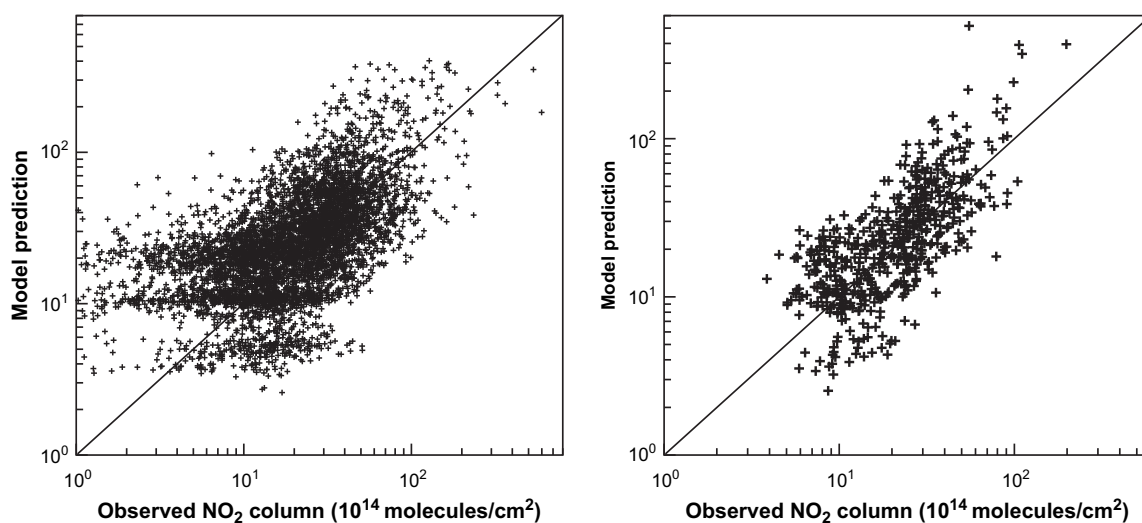


Fig. 4. Comparison between SCIAMACHY NO₂ columns and “model counterparts”, before (left) and after (right) averaging in each grid cell. “Model counterparts” were generated by assuming all the observations were measured on July 20, 2004.

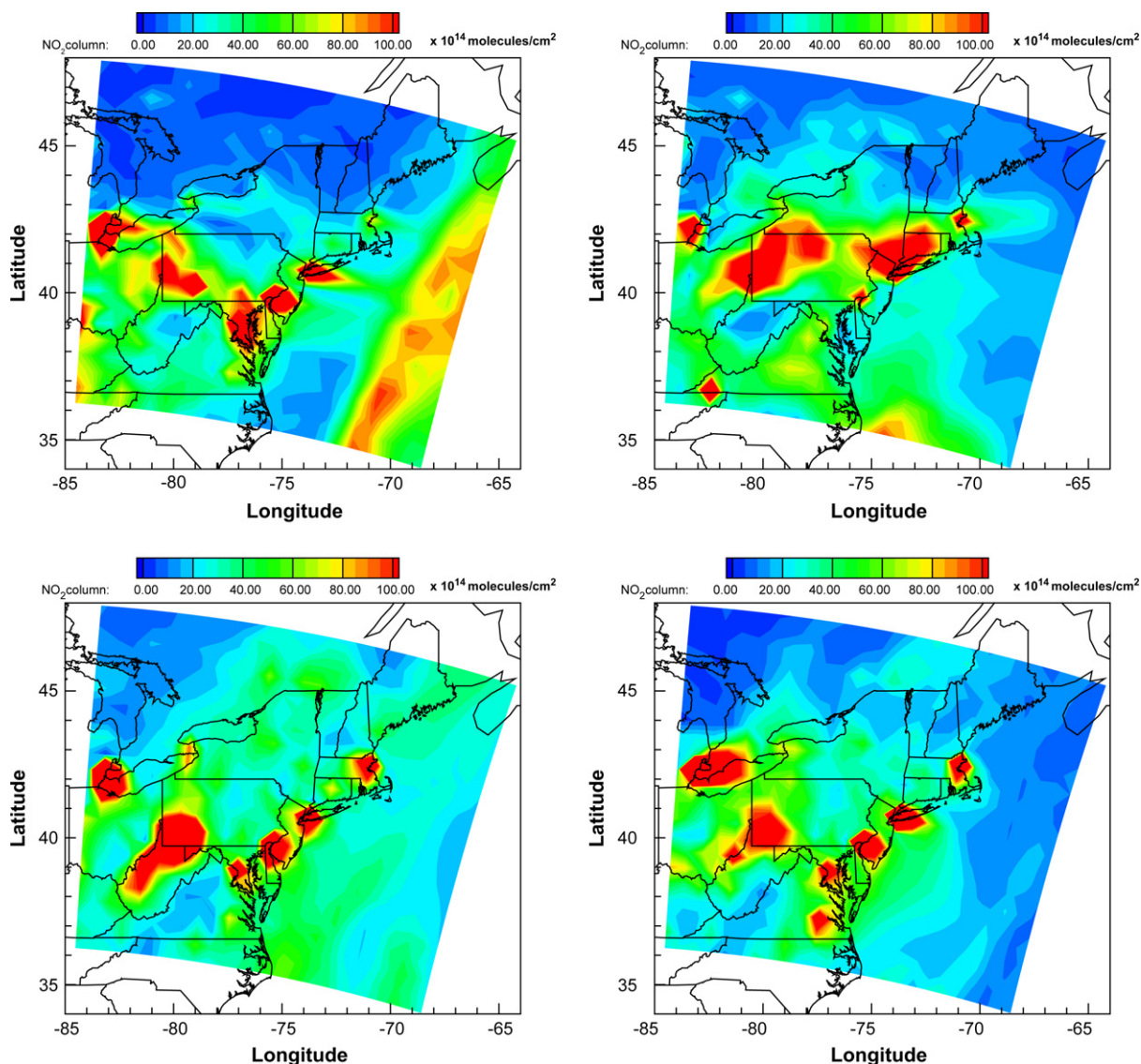


Fig. 5. Modeled NO₂ columns on July 17, 18, 19, and 20 respectively.

the initial ozone states. The most recent work by Elbern et al. (2007) studied the effect of combining both emission rate and initial state as control variables. Also note that we chose emission scaling factors ϵ instead of the emission rates as control parameters (see Hakami et al. (2005); Pan et al. (2007) for detail). However, the linear penalty applied to the emission scaling factors is prone to low-biased results. To avoid the problem, a logarithmic function of the scaling factors could be introduced into the cost functional.

Appendix A illustrates the association between emission sensitivity and adjoint variables through the “continuous adjoint” approach. In our application, the “discrete adjoint” approach is implemented to assure consistency. This is briefly described in Appendix B. More discussion on “continuous adjoint” and “discrete adjoint” can be found in Sandu et al. (2005).

4. Results

4.1. Results without assimilation

First we included all the measurements and assumed the two-month observations were measured on July 20, 2004. Fig. 4 shows the

comparison between the SCIAMACHY NO₂ columns and the “model counterparts” on July 20, 2004. It is seen that the model mostly overestimates the low NO₂ column values ($<10^5$ molecules cm⁻²). Then we considered the pseudo-columns which were generated by averaging multiple observations during the two-month period at each grid cell. Fig. 4 shows a good agreement between such pseudo-observations and their “model counterparts”. Note that the low NO₂ column values were effectively removed after the averaging for the pseudo-observations.

Fig. 5 shows model predictions of NO₂ columns on July 17 (Saturday), 18 (Sunday), 19 (Monday), and 20 (Tuesday),

Table 1

Assessment of NO₂ column predictions on four different days (July 17–20, 2004) against the SCIAMACHY pseudo-columns. Units of bias, mean error, and RMS error are 10¹⁴ molecules cm⁻².

Date	Bias	Mean error	RMS error	Correlation coefficient
July 17, 2004	13.6	25.2	41.4	0.336
July 18, 2004	8.7	18.1	29.6	0.491
July 19, 2004	11.7	17.7	28.9	0.587
July 20, 2004	6.7	14.6	33.4	0.673

Table 2

Descriptions of data assimilation test cases.

Case	Assimilation window	Assimilated observation	Control variables
EM01	0000–2400 UT, July 20, 2004	NO ₂ column	NOx emission
EM02	0000–2400 UT, July 19, 2004	NO ₂ column	NOx emission
IE01	0000–2400 UT, July 20, 2004	NO ₂ column	Init O ₃ + NOx emission
IE02	0000–2400 UT, July 20, 2004	NO ₂ column, O ₃	Init O ₃ + NOx emission

Init: initial.

respectively. The NO₂ columns were constructed at the same time of the day when the measurement was made. The current emission scheme differentiates Saturdays and Sundays from weekdays, i.e., it has 3 different temporal daily profiles. Since the NO₂ columns are dominated by the lower level NO₂ concentrations, the different NOx daily emission profiles generated significantly different NO₂ columns. It is shown in Fig. 5 that NO₂ predictions on July 17 and 18 are dramatically different from those predicted during the weekdays. The differences between July 19 and 20 predictions are relatively small, albeit apparent. The distribution of NO₂ column predictions on the weekdays resemble that of the SCIAMACHY observations shown in Fig. 3. Table 1 shows that the model overestimates the NO₂ columns for all four days. Predictions on July 20, 2004 gives the best overall agreement with the SCIAMACHY observations, showing a small bias of 6.7×10^{14} molecules cm⁻², and correlation coefficient as 0.673.

4.2. Assimilation results

The emission inversion tests are listed in Table 2. In all four tests, the NOx emission scaling factors are adjusted. Considering the different nature of the two major NOx sources, transportation and power plants, we adjust the surface and elevated (above the first level) NOx emissions with two different sets of emission scaling factors. No temporal variation is assumed for the scaling factors. That is, the diurnal variations of the original emissions are preserved. In the emission inversion, the valid range of the emission scaling factors is set to be between 0.1 and 10.0.

In case EM01, NO₂ columns are assimilated on July 20, 2004 with a 24-h time window. The distributions of the NOx emission scaling

Table 3Data assimilation results. Units of bias and RMS error for NO₂ columns are 10¹⁴ molecules cm⁻².

Case	Emission ratio (adjusted/original)			NO ₂ columns		
	Surface	Elevated	Total	Bias	RMS error	Correlation coefficients
EM01	0.934	0.879	0.920	0.6	12.2	0.819
EM02	0.936	0.879	0.922	5.7	15.9	0.819
IE01	0.973	0.876	0.949	-0.9	12.1	0.832
IE02	0.992	0.911	0.972	3.6	15.1	0.794

factors at the surface and upper levels are shown in Fig. 6. In most of the domain there is little NOx emission adjustment, indicated by the regions with the emission scaling factors close to one. Close to the area where the states of Ohio, West Virginia, and Pennsylvania join each other hereinafter referred as the OWP area, both surface and elevated emissions show downward adjustment to alleviate the model overestimation (see Figs. 3 and 5). Similar emission reductions are found at Detroit and Washington DC areas for both surface and elevated emissions as well. At the surface, there are several other locations with NOx emissions adjusted up or down. However, these locations are often not associated with large NOx emission sources. To show the overall emission adjustment in the domain, we multiply the emission scaling factors with their base emission rates. The results are shown in Table 3. It shows that the elevated emissions are reduced by 12.9% and the surface emissions are reduced by only 6.6%. Combined together, the total NOx emissions are reduced by 8.0% after assimilating the SCIAMACHY data. After the emission adjustment, the model results of NO₂ columns improve significantly. As shown in Tables 1 and 3, the bias is reduced from 6.7×10^{14} molecules cm⁻² to 0.6×10^{14} molecules cm⁻², and root-mean-square (RMS) error is reduced from 33.4×10^{14} molecules cm⁻² to 12.2×10^{14} molecules cm⁻². The correlation between the model and observation also improves, with correlation coefficient increased from 0.673 to 0.819.

The setup of case EM02 is same as case EM01, except that the assimilation time window is shifted one day earlier. Note that there are not only changes in the meteorological fields, but also differences in the atmospheric chemistry states. The distributions of the NOx emission scaling factors at the surface and upper levels are

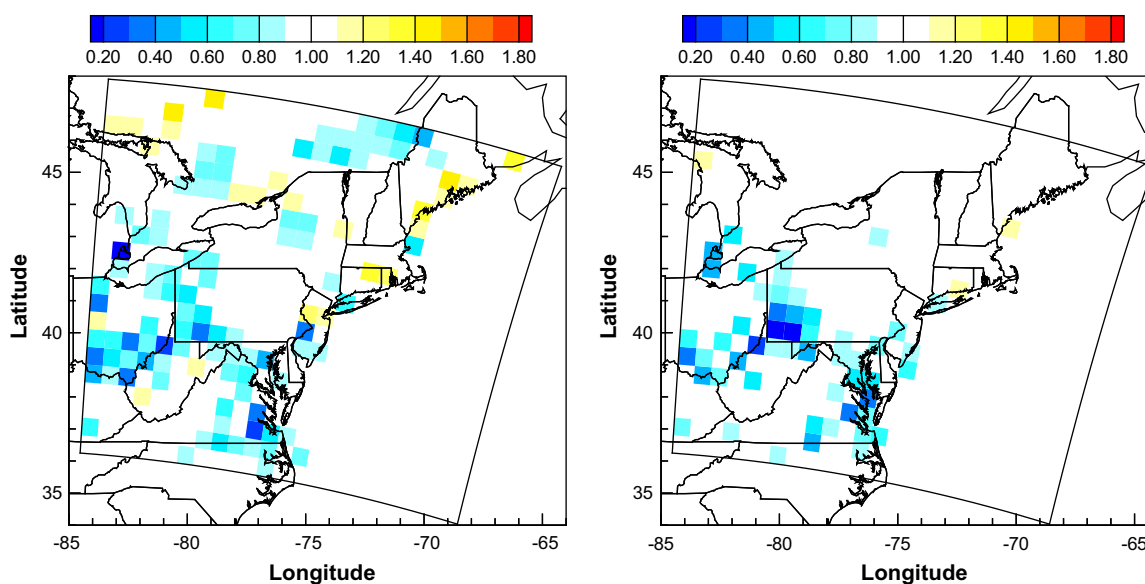


Fig. 6. Distributions of NOx emission scaling factors from Case EM01. Left: surface; right: upper levels.

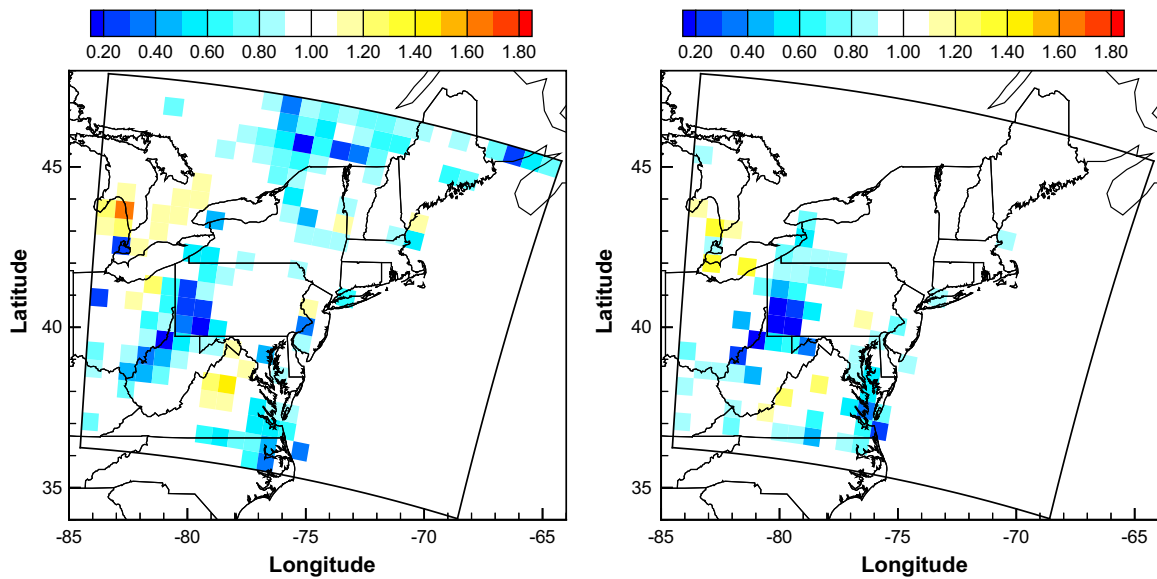


Fig. 7. Distributions of NO_x emission scaling factors from Case EM02. Left: surface; right: upper levels.

shown in Fig. 7. Emission reductions are seen around the OWP area and Washington DC in both surface and upper levels, similar as case EM01 shown in Fig. 6. However, the emission reduction in the OWP area for case EM02 is greater than that in case EM01. For the surface NO_x emissions, there are differences in the direction of the adjustments at several locations, such as the northeast and north-west corners of the domain. For the elevated emissions, results of the two cases resemble each other except for slight differences in northern Virginia and western Erie lake areas. The emission changes over the whole domain after the adjustment for case EM02 are very close to case EM01, especially for the emissions at the upper levels, with both cases showing a 12.1% reduction over the domain.

In cases EM01 and EM02, only the NO_x emissions are adjusted to fit the model predictions of the SCIAMACHY NO₂ columns. This approach assumes that the only source of error is the emission, thus

it attempts to minimize the model prediction errors by adjusting emissions only. With significant uncertainties in many other parameters, such as initial and boundary conditions, reaction rates, and meteorological fields, the emission adjustments may yield faulty results due to the errors in the other model parameters. In cases IE01 and IE02 which are listed in Table 2, we extend the emission inversion to include the simultaneous adjustment of additional parameters. Adjoint sensitivity shows that NO₂ columns are more sensitive to the initial concentrations of O₃ than those of the other species, including NO₂. It is probably because NO₂ plays a key role in the troposphere ozone chemistry and NO₂ has a short lifetime. We chose to add initial ozone concentrations as control variables.

Fig. 8 shows the distributions of the NO_x emission scaling factors from case IE01. Great similarity is found between Figs. 6 and 8, especially for the elevated emissions. At the surface, the magnitude

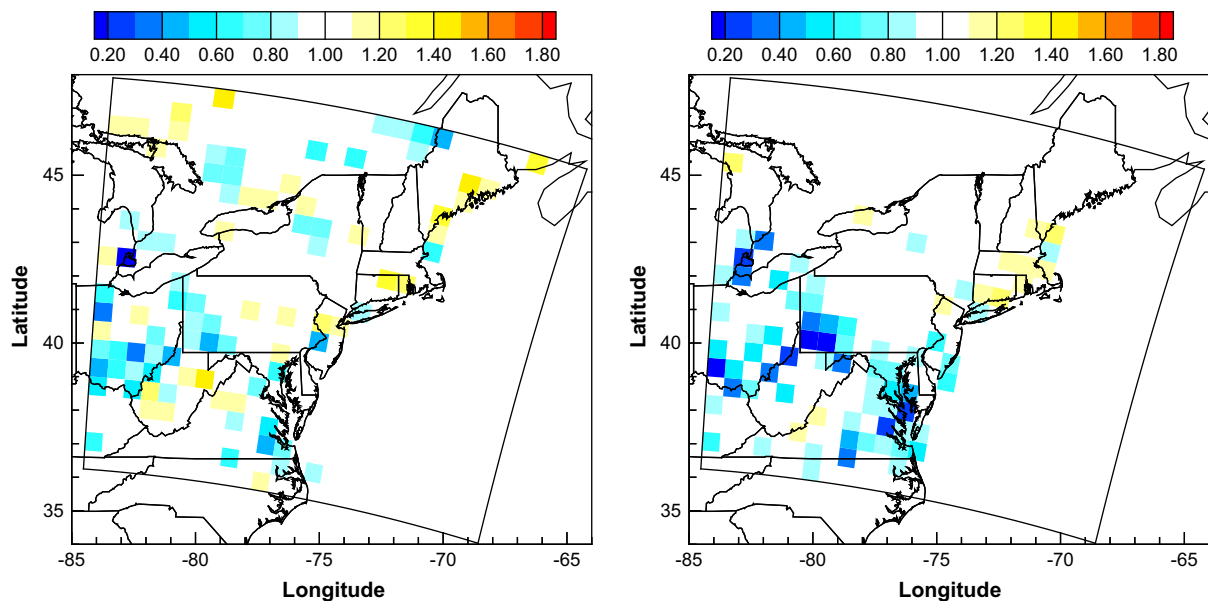


Fig. 8. Distributions of NO₂ emission scaling factors from case IE01. Left: surface; right: upper levels.

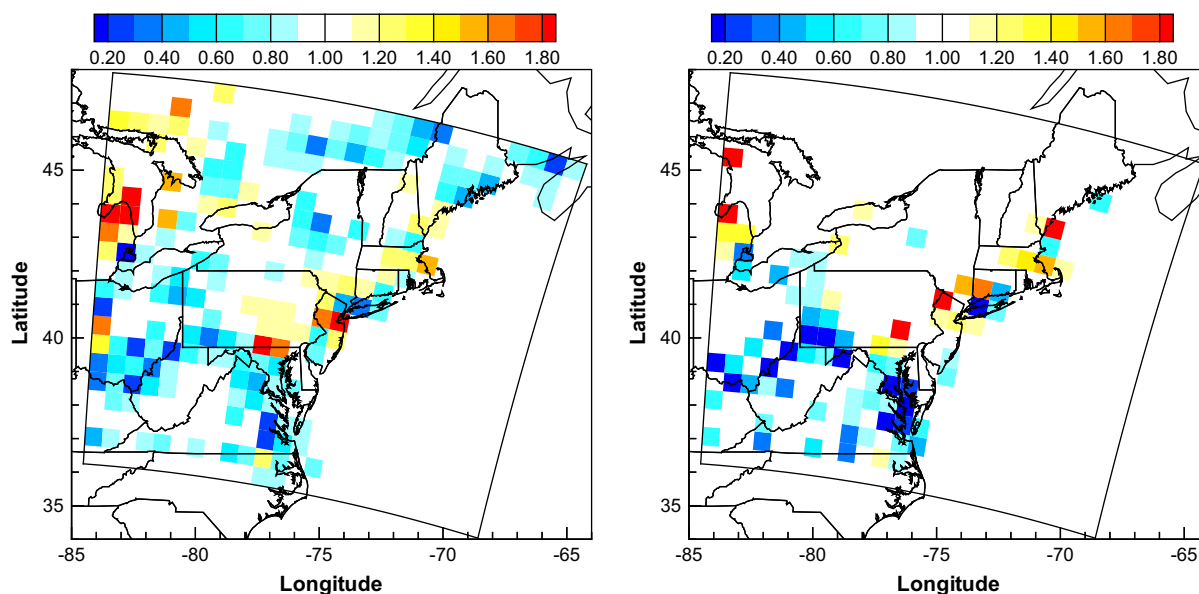


Fig. 9. Distributions of NO₂ emission scaling factors from Case IE02. Left: surface; right: upper levels.

of the emission adjustment tends to be smaller than for the case EM01 in most regions. As listed in Table 3, the total emission reduction at surface over the computational domain (2.7%) is less than half of case EM01 (6.6%). The emission reduction for IE01 at the upper levels (12.4%) is close to the result of case EM01 (12.1%). By allowing additional parameters to be adjusted, the model predictions of NO₂ are slightly better than case EM01, as indicated by model bias, RMS error, and correlation coefficient listed in Table 3.

In case IE01, it is found that allowing the NO₂ column observations to impact both the emission scaling factors and the initial O₃ improves the NO₂ predictions. We also explored whether assimilating additional observations would improve the results. In case IE02, ozone observations from various platforms on July 20, 2004 (see Chai et al., 2007 for details) are added to the observation set assimilated. Same as case IE01, both the emission scaling factors and the initial O₃ concentrations are treated as control variables. Fig. 9 shows the distributions of NO_x emission scaling factors yielded from case IE02, which are quite different from the previous cases. However, the emission reduction in the OWP and DC areas is consistent with the previous tests. Case IE02 results show that the NO_x emissions at several grid cells need to be doubled in order for the model to match the additional ozone observations. After integrating over the computational domain, we see little change in the NO_x emissions at the surface (0.8% in reduction). At the upper levels, the emission reduction of 8.9% over the domain is close to the previous cases. Compared with cases IE01 and EM01 (see Table 3), IE02 generates NO₂ predictions with worse bias (3.6×10^{14} molecules cm⁻²), larger RMS error (15.1×10^{14} molecules cm⁻²), and smaller correlation coefficient (0.794). This suggests that the additional O₃ observations do not help constraining the NO_x emissions. It is probably due to the high uncertainty in other parameters involved in the ozone chemistry, such as the emissions of volatile organic compounds (VOCs).

5. Summary

In a “top-down” approach, SCIAMACHY NO₂ column data in the summer of 2004 are assimilated into a chemical transport model (CTM), STEM. We demonstrate that the four-dimensional variational (4D-Var) approach allows a more general framework in emission inversion. In this general setup, more uncertain model parameters can be adjusted in addition to the emission fields.

Observations of different species in various formats can also be used to constrain the inverse problem.

The test cases show that the emission inversion results are sensitive to the problem setup. Emission scaling factors from the last case where both ozone observations and NO₂ column data are assimilated while allowing initial ozone and NO_x emissions to be adjusted are very different from the other cases. It is probably not beneficial to add ozone observations to constrain the NO_x emissions because of the great uncertainties associated with VOCs.

When only NO₂ column data are assimilated, adding initial ozone concentrations as control variables to be adjusted generates less adjustment in NO_x emissions, especially for the surface emissions. All the cases show consistent results over the Ohio valley region and Washington, District of Columbia area, revealing the NO_x emission reduction. With emissions at surface and upper levels adjusted separately, we found the results at upper levels are quite robust. The elevated NO_x emission reduction results from four test cases range from 8.9% to 11.4%, indicating the power plant NO_x emission reduction from 2001 to 2004. Stavrou et al. (2008) reported their inferred posterior NO_x emissions are decreased by 35% between July 1997 and 2006 in the Ohio River Valley, with annual change rate of -4.3% year⁻¹ in summertime. This agrees well with our results.

While SCIAMACHY satellite observations provide more than adequate data for global model emission inversion, their temporal and spatial resolutions are lacking for a regional model application to resolve detailed grid-based emission inversion. Ignoring the daily variability, we stacked together the NO₂ columns in two months to generate a pseudo-observation set that has the two-month mean at each grid cell. Such pseudo-observations do not reflect the daily variations in chemistry and physics of the troposphere. Also note that the satellite observations are usually least sensitive to the boundary layer where most of the emissions occur. In addition, the 24-h assimilation time window chosen for the NO_x emission inversion tests has its drawback as well. Although we showed that the NO_x emission inversion tests using two different days generated very similar results, a full 2-month inversion wherein NO₂ columns from each day are assimilated separately is still preferable. While our main focus here is on the formulating of the emission inversion problem, we plan to apply such pseudo-observations as well as the original data over a larger domain for an

extended time period in the future. Such emission inversion results will be able to provide more valuable information to evaluate and improve the “bottom-up” emission inventories. In the end, we want to emphasize that the current emission inversion formulation can be easily applied to other types of measurements, although here we focus on the emission inversion using the SCIAMACHY NO₂ columns.

Acknowledgments

The authors gratefully thank NASA, NOAA, and the National Science Foundation for their support grants.

Appendix A. Emission sensitivity via continuous adjoint

Here we first consider a simple one dimensional problem involving only one species. By assuming constant air density, and ignoring the advection and reaction terms, the transport equation is further simplified and becomes

$$\frac{\partial c}{\partial t} = \frac{\partial}{\partial z} \left(K \frac{\partial c}{\partial z} \right) + E(z, t) \quad (3)$$

where $c = c(z, t)$ and $z \in (0, L)$, $t \in (0, T)$. As we only aim to illustrate how the emission sensitivity associates with the adjoint variables, instead of a cost functional in the least square form as in equation (2), we define a general response functional as

$$J = \frac{1}{LT} \int_0^L \int_0^T g(z, t) dt dz \quad (4)$$

To derive the adjoint equation, we introduce the Lagrange multiplier $\lambda_c(z, t)$. Multiply equation (3) with it and integrate over computational domain (a factor of 1/L is added). Subtract the result from equation (4), we get

$$J' = J - \frac{1}{L} \int_0^L \int_0^T \lambda_c \left[\frac{\partial c}{\partial t} - \frac{\partial}{\partial z} \left(K \frac{\partial c}{\partial z} \right) - E(z, t) \right] dt dz \quad (5)$$

The variation of equation (5) yields

$$\begin{aligned} \delta J' = \delta J - \frac{1}{L} \int_0^L \int_0^T \delta \lambda_c \left[\frac{\partial c}{\partial t} - \frac{\partial}{\partial z} \left(K \frac{\partial c}{\partial z} \right) - E(z, t) \right] dt dz \\ - \frac{1}{L} \int_0^L \int_0^T \lambda_c \left[\frac{\partial \delta c}{\partial t} - \frac{\partial}{\partial z} \left(K \frac{\partial \delta c}{\partial z} \right) - \delta E(z, t) \right] dt dz \end{aligned} \quad (6)$$

Integrating by parts gives

$$\begin{aligned} \delta J' = \frac{1}{LT} \int_0^L \int_0^T \delta g(z, t) dt dz - \frac{1}{L} \int_0^L \int_0^T \delta \lambda_c \left[\frac{\partial c}{\partial t} - \frac{\partial}{\partial z} \left(K \frac{\partial c}{\partial z} \right) \right. \\ \left. - E(z, t) \right] dt dz - \frac{1}{L} \int_0^L \int_0^T \delta c \left[- \frac{\partial \lambda_c}{\partial t} - \frac{\partial}{\partial z} \left(K \frac{\partial \lambda_c}{\partial z} \right) \right] dt dz \\ - \frac{1}{L} \int_0^L \left[- K \lambda_c \frac{\partial \delta c}{\partial z} + K \delta c \frac{\partial \lambda_c}{\partial z} \right]_0^L dt - \frac{1}{L} \int_0^L [\lambda_c \delta c]_{t=0} dz \\ + \frac{1}{L} \int_0^L [\lambda_c \delta c]_{t=T} dz + \frac{1}{L} \int_0^L \int_0^T \lambda_c \delta E(z, t) dt dz \end{aligned} \quad (7)$$

The second term on the right-hand side vanishes as the state variable satisfies equation (3). Combine the first and the third terms and force them to vanish. This gives the adjoint equation

$$\frac{\partial \lambda_c}{\partial t} = - \frac{\partial}{\partial z} \left(K \frac{\partial \lambda_c}{\partial z} \right) - \frac{1}{T} \frac{\partial g}{\partial c} \quad (8)$$

The fourth term would vanish with proper boundary conditions (e.g., $\lambda_c = 0$ at Dirichlet boundaries). Forcing the fifth term to be zero gives the initial condition for the adjoint variable λ_c at $t = T$ as

$$\lambda_c(z, T) = 0 \quad (9)$$

Then equation (7) becomes

$$\delta J' = \frac{1}{L} \int_0^L [\lambda_c \delta c]_{t=0} dz + \frac{1}{LT} \int_0^L \int_0^T T \lambda_c \delta E(z, t) dt dz \quad (10)$$

This provides the variational sensitivity information for both the initial and emission functions.

$$\frac{\delta J'}{\delta c(z, t = 0)} = \lambda_c(z, t = 0), \frac{\delta J'}{\delta E(z, t)} = T \lambda_c(z, t) \quad (11)$$

If we introduce emission scaling factors ε as

$$\varepsilon(z) = \frac{E(z, t)}{E_0(z, t)} \quad (12)$$

Note $\varepsilon(z)$ does not vary in time. The last term in equation (7) would become

$$\frac{1}{L} \int_0^L \left(\int_0^T \lambda_c E_0(z, t) dt \right) \delta \varepsilon(z) dz \quad (13)$$

Thus, the sensitivity of the response function to the emission scaling factor has the following form

$$\frac{\delta J'}{\delta \varepsilon(z)} = \int_0^T \lambda_c E_0(z, t) dt \quad (14)$$

Without detail, here we give the emission sensitivity for species i in a four-dimensional air quality model,

$$\frac{\delta J'}{\delta \varepsilon_i(x, y, z)} = \int_0^T \lambda_{c_i}(x, y, z) E_0(x, y, z, t) dt \quad (15)$$

In the current study, emission rates are adjusted separately using two sets of 2-D functions, $\varepsilon^s(x, y)$ for the surface and $\varepsilon^e(x, y)$ for higher levels.

$$\frac{\delta J'}{\delta \varepsilon_i^s(x, y)} = \int_0^T \lambda_{c_i}(x, y, z) \frac{q_0(x, y, t)}{\Delta z_1} dt \quad (16)$$

$$\frac{\delta J'}{\delta \varepsilon_i^e(x, y)} = \frac{1}{z_{\text{top}} - z_1} \int_{z_1}^{z_{\text{top}}} \int_0^T \lambda_{c_i}(x, y, z) E_0(x, y, z, t) dt dz \quad (17)$$

where Δz_1 is the depth of the first layer. z_1 and z_{top} are the height of the first and top layer, respectively. Note that the surface area emission $q_0(x, y, t)$ includes the first level volume emission rate, i.e.

$$q_0(x, y, t) = q_0^{\text{surface}}(x, y, t) + \int_0^{z_1} E_0(x, y, z, t) dz \quad (18)$$

Appendix B. Emission sensitivity via discrete adjoint

As operator-splitting technique is implemented in solving equation (1), the emission sensitivity is only directly associated with vertical transport. Using Crank–Nicholson time stepping for the concentrations and forward Euler for boundaries and the surface emissions, the forward discrete model evolving the concentration column vector C_i from time step n to $n + 1$ for vertical transport reads

$$C_i^{n+1} = \left(I - \frac{\Delta t}{2} A(t^{n+1}) \right)^{-1} \left[\left(I + \frac{\Delta t}{2} A(t^n) \right) C_i^n + \Delta t \left(B(t^n) e_N + \sum_{j=2}^N E_i^j(t^n) e_j + \frac{q_i(t^n)}{\Delta z_1} e_1 \right) \right] \quad (19)$$

where matrix A depends on the wind field, the diffusion tensor, and the air density. B is a scalar that accounts for the top boundary. e_j is the j th column of the identity matrix. The adjoint sensitivity with respect to emission rates can be calculated as

$$\begin{aligned} \frac{\partial J}{\partial q_i(t^n)} &= \left(\frac{\partial C_i^{n+1}}{\partial q_i(t^n)} \right)^T \cdot \left(\frac{\partial J}{\partial C_i^{n+1}} \right) = \left(\frac{\partial C_i^{n+1}}{\partial q_i(t^n)} \right)^T \cdot \lambda_i^{n+1} \\ &= \frac{1}{\Delta z_1} e_1^T \left(I - \frac{\Delta t}{2} A^T(t^{n+1}) \right)^{-1} \lambda_i^{n+1} \cdot \Delta t \end{aligned} \quad (20)$$

$$\begin{aligned} \frac{\partial J}{\partial E_i^j(t^n)} &= \left(\frac{\partial C_i^{n+1}}{\partial E_i^j(t^n)} \right)^T \cdot \left(\frac{\partial J}{\partial C_i^{n+1}} \right) = \left(\frac{\partial C_i^{n+1}}{\partial E_i^j(t^n)} \right)^T \cdot \lambda_i^{n+1} \\ &= e_j^T \left(I - \frac{\Delta t}{2} A^T(t^{n+1}) \right)^{-1} \lambda_i^{n+1} \cdot \Delta t \end{aligned} \quad (21)$$

Since the vector $(I - (\Delta t/2)A^T(t^{n+1}))^{-1} \lambda_i^{n+1}$ is already computed during the update of λ , there is little additional cost to calculate the emission sensitivity. If we choose the non-time-varying emission scaling factors ε_i as control variables, their sensitivities can be written as

$$\frac{\partial J}{\partial \varepsilon_i^s} = \sum_{n=0}^{N_t-1} \left[\frac{1}{\Delta z_1} e_1^T \left(I - \frac{\Delta t}{2} A^T(t^{n+1}) \right)^{-1} \lambda_i^{n+1} q_{i0}(t^n) \Delta t \right] \quad (22)$$

$$\frac{\partial J}{\partial \varepsilon_i^e} = \sum_{n=0}^{N_t-1} \sum_{j=2}^{N_z} \left[e_j^T \left(I - \frac{\Delta t}{2} A^T(t^{n+1}) \right)^{-1} \lambda_i^{n+1} E_{i0}^j(t^n) \Delta t \right] \quad (23)$$

where N_t and N_z are total number of time steps and vertical levels, respectively.

References

Boersma, K.F., Jacob, D.J., Bucsel, E.J., Perring, A.E., Dirksen, R., van der A, R.J., Yantosca, R.M., Park, R.J., Wenig, M.O., Bertram, T.H., Cohen, R.C., 2008. Validation of OMI tropospheric NO₂ observations during INTEX-B and application to constrain NO_x emissions over the eastern United States and Mexico. *Atmos. Environ.* 42, 4480–4497.

Bovensmann, H., Burrows, J.P., Buchwitz, M., Frerick, J., Nol, S., Rozanov, V.V., 1999. SCIAMACHY: mission objectives and measurement modes. *J. Atmos. Sci.* 56 (2), 127–150.

Burrows, J.P., Weber, M., Buchwitz, M., Rozanov, V., Ladstätter-Weissenmayer, A., Richter, A., Debeek, R., Hoogen, R., Bramstedt, K., Eichmann, K.-U., 1999. The global ozone monitoring experiment (GOME): mission concept and first scientific results. *J. Atmos. Sci.* 56 (2), 151–175.

Carter, W., May 2000. Documentation of the SAPRC-99 Chemical Mechanism for VOC Reactivity Assessment. Tech. Rep. 92–329. California Air Resources Board Contract.

Chai, T., Carmichael, G.R., Sandu, A., Tang, Y., Daescu, D.N., 2006. Chemical data assimilation of transport and chemical evolution over the Pacific (TRACE-P) aircraft measurements. *J. Geophys. Res.* 111 (D02301). doi:10.1029/2005JD005883.

Chai, T., Carmichael, G.R., Tang, Y., Sandu, A., Hardesty, M., Pilewskie, P., Whitlow, S., Brown, E.V., Avery, M.A., Nédélec, P., Merrill, J.T., Thompson, A.M., Williams, E., 2007. Four-dimensional data assimilation experiments with International

Consortium for Atmospheric Research on Transport and Transformation ozone measurements. *J. Geophys. Res.* 112 (D12S15). doi:10.1029/2006JD007763.

Elbern, H., Strunk, A., Schmidt, H., Talagrand, O., 2007. Emission rate and chemical state estimation by 4-dimensional variational inversion. *Atmos. Chem. Phys.* 7, 3749–3769.

Frost, G.J., McKeen, S.A., Trainer, M., Ryerson, T.B., Neuman, J.A., Roberts, J.M., Swanson, A., Holloway, J.S., Sueper, D.T., Fortin, T., Parrish, D.D., Fehsenfeld, F.C., Flocke, F., Peckham, S.E., Grell, G.A., Kowal, D., Cartwright, J., Auerbach, N., Habermann, T., 2006. Effects of changing power plant NO_x emissions on ozone in the eastern United States: proof of concept. *J. Geophys. Res.* 111 (D12) Art. No. D12306.

Hakami, A., Henze, D., Seinfeld, J.H., Chai, T., Tang, Y., Carmichael, G.R., Sandu, A., 2005. Adjoint inverse modeling of black carbon during the Asian Pacific Regional Aerosol Characterization Experiment. *J. Geophys. Res.* 110 (D14301). doi:10.1029/2004JD005671.

Henze, D.K., Seinfeld, J.H., Shindell, D.T., 2008. Inverse modeling and mapping US air quality influences of inorganic PM_{2.5} precursor emissions using the adjoint of GEOS-Chem. *Atmos. Chem. Phys. Discuss.* 8, 15031–15099.

Horowitz, L.W., Walters, S., Mauzerall, D.L., Emmons, L.K., Rasch, P.J., Granier, C., Tie, X., Lamarque, J.F., Schultz, M., Tyndall, G.S., Orlando, J.J., Brasseur, G.P., 2003. A global simulation of tropospheric ozone and related tracers: description and evaluation of MOZART, version 2. *J. Geophys. Res.* 108 (D24) Art. No. 4784.

Jaeglé, L., Steinberger, L., Martin, R.V., Chance, K., 2005. Global partitioning of NO_x sources using satellite observations: relative roles of fossil fuel combustion, biomass burning and soil emissions. *Faraday Discuss.* 130, 407–423.

Martin, R.V., Jacob, D.J., Chance, K., Kurosu, T.P., Palmer, P.L., Evans, M.J., 2003. Global inventory of nitrogen oxide emissions constrained by space-based observations of NO₂ columns. *J. Geophys. Res.* 108 (D17). doi:10.1029/2003JD003453.

Müller, J.-F., Stavrakou, T., 2005. Inversion of CO and NO_x emissions using the adjoint of the IMAGES model. *Atmos. Chem. Phys.* 5, 1157–1186.

Napelnenok, S.L., Pinder, R.W., Gilliland, A.B., Martin, R.V., 2008. A method for evaluating spatially-resolved NO_x emissions using Kalman filter inversion, direct sensitivities, and space-based NO₂ observations. *Atmos. Chem. Phys.* 8, 5603–5614.

Palmer, P., Jacob, D., Jones, D., Heald, C., Yantosca, R., Logan, J., Sachse, G., Streets, D., 2003. Inverting for emissions of carbon monoxide from Asia using aircraft observations over the western Pacific. *J. Geophys. Res.* 108 (D21) Art. No. 8821.

Pan, L., Chai, T., Carmichael, G., Tang, Y., Streets, D., Woo, J., Friedli, H.R., Radke, L.F., 2007. Top-down estimate of mercury emissions in china using four-dimensional variational data assimilation. *Atmos. Environ.* 41 (13), 2804–2819.

Pétron, G., Granier, C., Khattatov, B., Lamarque, J.-F., Yudin, V., Müller, J.-F., 2002. Inverse modeling of carbon monoxide surface emissions using climate monitoring and diagnostics laboratory network observations. *J. Geophys. Res.* 107 (D24) Art. No. 4761.

Richter, A., Burrows, J.P., 2002. Retrieval of tropospheric NO₂ from GOME measurements. *Adv. Space Res.* 29 (11), 1673–1683.

Richter, A., Burrows, J.P., Nüß, H., Granier, C., Niemeier, U., 2005. Increase in tropospheric nitrogen dioxide over China observed from space. *Nature* 437, 129–132. doi:10.1038/nature04092.

Sandu, A., Daescu, D., Carmichael, G.R., Chai, T., 2005. Adjoint sensitivity analysis of regional air quality models. *J. Comput. Phys.* 204 (1), 222–252.

Singh, H.B., Brune, W.H., Crawford, J.H., Jacob, D.J., Russell, P.B., 2006. Overview of the summer 2004 Intercontinental Chemical Transport Experiment-North America (INTEX-A). *J. Geophys. Res.* 111 (D24S01). doi:10.1029/2006JD007905.

Stavrakou, T., Müller, J.-F., 2006. Grid-based versus big region approach for inverting CO emissions using Measurement of Pollution in the Troposphere (MOPITT) data. *J. Geophys. Res.* 111 (D15304). doi:10.1029/2005JD006896.

Stavrakou, T., Müller, J.-F., Boersma, F., Smedt, I.D., van der A, R.J., 2008. Assessing the distribution and growth rates of NO_x emission sources by inverting a 10-year record of NO₂ satellite columns. *Geophys. Res. Lett.* 35 (L10801). doi:10.1029/2008GL033521.

Talagrand, O., Courtier, P., 1987. Variational assimilation of meteorological observations with the adjoint vorticity equation. I: theory. *Quart. J. R. Meteorol. Soc.* 113, 1311–1328.

Tang, Y., Carmichael, G., Horowitz, L., Uno, I., Woo, J., Streets, D., Dabdub, D., Kurata, G., Sandu, A., Allan, J., Atlas, E., Flocke, F., Huey, L., Jakoubek, R., Millet, D., Quinn, P., Roberts, J., Worsnop, D., Goldstein, A., Donnelly, S., Schaufli, S., Stroud, V., Johnson, K., Avery, M., Singh, H., Apel, E., 2004. Multiscale simulations of tropospheric chemistry in the eastern Pacific and on the US west coast during spring 2002. *J. Geophys. Res.* 109 (D23) Art. No. D23S11.

Tang, Y., Carmichael, G., Thongboonchoo, N., Chai, T., Horowitz, L.W., Poerco, R.B., Al-Saadi, J.A., Pfister, G., Vukovich, M., Avery, M.A., Sachse, G.W., Ryerson, T.B., Holloway, J.S., Atlas, E.L., Flocke, F.M., Weber, R.J., Huey, L.G., Dibb, J.E., Streets, D.G., Brune, W.H., 2007. The influence of lateral and top boundary conditions on regional air quality prediction: a multi-scale study coupling regional and global chemical transport models. *J. Geophys. Res.* 112 (D10S18). doi:10.1029/2006JD007515.

Tang, Y., Carmichael, G., Uno, I., Woo, J., Kurata, G., Lefer, B., Shetter, R., Huang, H., Anderson, B., Avery, M., Clarke, A., Blake, D., 2003. Impacts of aerosols and clouds on photolysis frequencies and photochemistry during TRACE-P: 2. Three-dimensional study using a regional chemical transport model. *J. Geophys. Res.* 108 (D21) Art. No. 8822.

Wang, Y., McElroy, M., Wang, T., Palmer, P., 2004. Asian emissions of CO and NO_x: constraints from aircraft and Chinese station data. *J. Geophys. Res.* 109 (D24) Art. No. D24304.

Zhu, C., Byrd, R.H., Nocedal, J., 1997. L-BFGS-B – fortran routines for large scale bound constrained optimization. *ACM Trans. Math. Software* 23 (4), 550–560.